Cementitious cellular composites with auxetic behavior

Xu, Yading; Zhang, Hongzhi; Schlangen, Erik; Lukovic, Mladena; Šavija, Branko

DOI
10.1016/j.cemconcomp.2020.103624

Publication date
2020

Document Version
Final published version

Published in
Cement and Concrete Composites

Cement and Concrete Composites 111 (2020) 103624

Contents lists available at ScienceDirect

Cement and Concrete Composites

journal homepage: http://www.elsevier.com/locate/cemconcomp

Cementitious cellular composites with auxetic behavior

Yading Xu, Hongzhi Zhang *, Erik Schlangen, Mladena Luković, Branko Šavija

Faculty of Civil Engineering and Geosciences, Delft University of Technology, 2628 CN, Delft, the Netherlands

ARTICLE INFO

Keywords:
Auxetic material
Negative Poisson's ratio
Cementitious material
Cyclic loading

ABSTRACT

Auxetic behavior refers to material with negative Poisson's ratio. In this research, a new type of cementitious auxetic material is developed. A novel crack bridging auxetic mechanism is discovered which is in contrast with a local buckling mechanism commonly employed to trigger auxetic behavior. Taking advantage of 3D printing techniques, cementitious cellular composite (CCC) specimens with auxetic cellular structures were produced. Meanwhile, cementitious materials with different fiber content were used as constituent material. Uniaxial compression and cyclic loading tests were performed on the CCCs. Experiments show that with proper constituent material, CCCs can exhibit auxetic behavior which is induced by crack bridging process of the cementitious constituent material. In addition, strain hardening behavior can be identified in the stress-strain curve under uniaxial compression and consequently high specific energy absorption is obtained. Furthermore, 2.5% of reversible deformation which is significantly higher than conventional cementitious materials under cyclic loading is obtained within 25,000 cycles. Obvious fatigue damage is observed in the first 3000 cycles, afterwards signs of mechanical properties recovering can be found. The discovered auxetic mechanism indicates a new designing direction for brittle materials to achieve auxetic behaviors.

1. Introduction

Cementitious materials are the most widely used construction materials in the world due to their excellent properties and relatively low cost. Studies have shown that mechanical properties of cementitious materials depend not only on their constituent phases (e.g. properties of matrix [1–3], aggregates [4,5] and fibers [6,7]) but also the geometrical characteristics and spatial distribution of these constituents [8,9]. This is referred to as "micro-structure" or "meso-structure" of cementitious materials. In this sense, the cementitious materials mechanical behavior can be also regarded as structural behavior of a complex multi-constituent system. In the past several decades, intensive efforts have focused on configuring or modifying the micro/meso-structure of cementitious materials to improve their performance. For instance, optimizing the packing density [10–12], modifying the pore structure [13–15], modifying air void structure [16,17] and introducing new phases as reinforcement [18,19]. In all those cases, the material micro/meso-structure is chemically tailored which means that usually admixtures or additives are used to configure the mix proportions. Besides this traditional approach, physically architecting the micro-/meso-structure, namely distributing constituent cementitious materials with certain designed geometry, may enable another dimension of freedom for cementitious material design. For many other materials. architecting the material geometrical micro-/meso-structure has been proven to be a very efficient method to modify material properties: examples include polymers [20–23], metals [24–26] and ceramics [27,28]. However, architecting the geometrical structure of cementitious materials is seldomly reported: to the knowledge of the authors, the only study dealing with this topic was performed by Moini et al. [29] who tailored the meso-structure of cement paste by 3D printing. Various cellular structures have already been studied and used in engineering practice. Examples include Kagome structures with high relative fracture toughness [30,31], octet lattices with high relative strength [32,33] and auxetic structures with high impact resistance [34–37]. Among those geometries, auxetic structures are of particular interest for cementitious materials because of their excellent mechanical properties which might be applied in many engineering practices.

The term "auxetic", coined by Evans in 1991 [38], refers to a material possessing a negative Poisson's ratio. This means that the material exhibits lateral contraction or expansion when compressed or stretched vertically, respectively. This unusual behavior gives auxetic materials extraordinary mechanical properties: enhanced indentation resistance [39–41], high specific energy absorption [42–44], and high shear resistance [42,45]. Unlike the high strength concrete used for common

* Corresponding author.
E-mail address: hzzhang@sdu.edu.cn (H. Zhang).

https://doi.org/10.1016/j.cemconcomp.2020.103624
Received 31 October 2019; Received in revised form 3 April 2020; Accepted 5 April 2020
Available online 11 April 2020

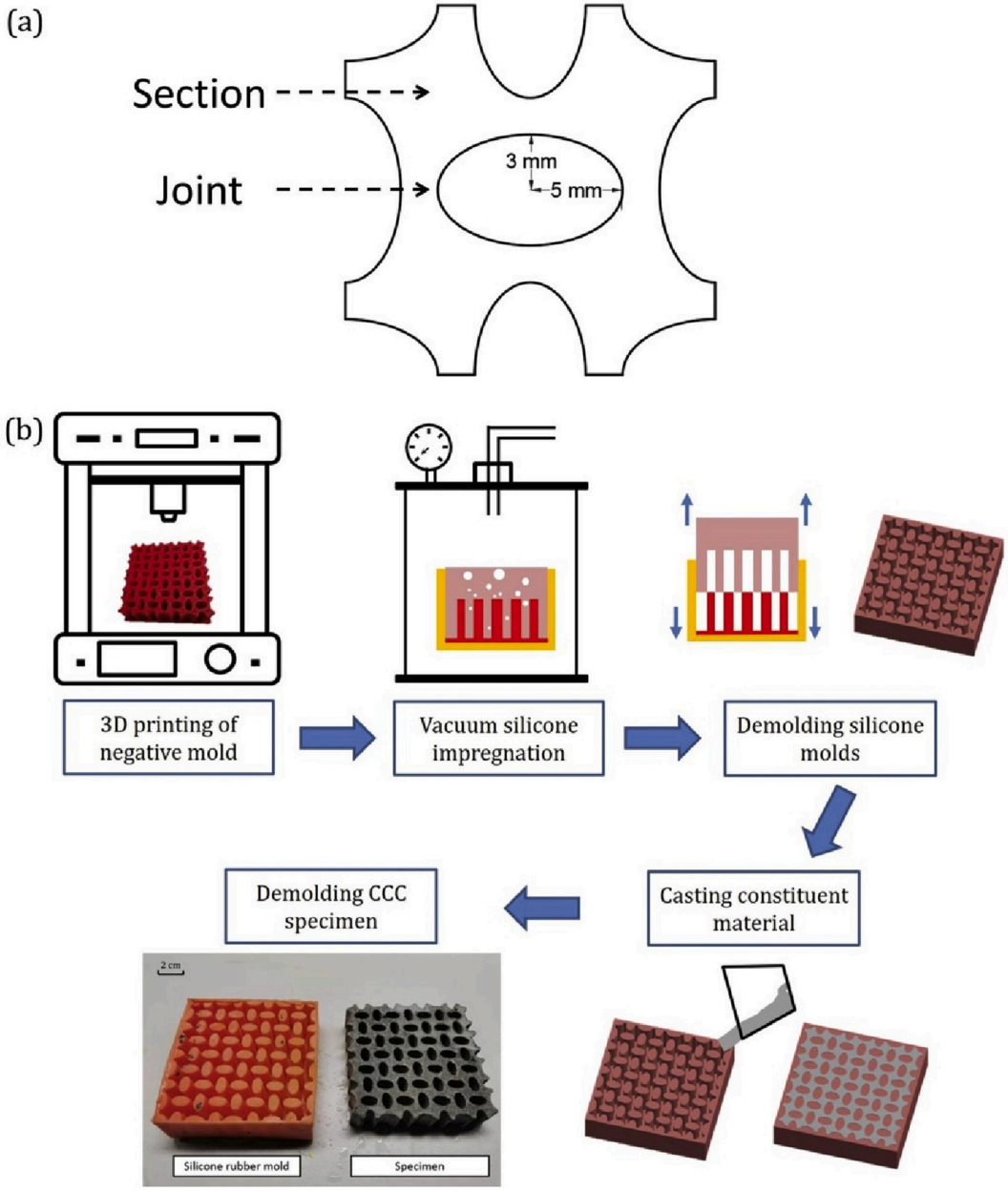

Fig. 1. (a) a unit cell of the cellular structure with $a = 5$ mm and $b = 3$ mm, adopted from Ref. [58]; (b) the so called "indirect 3D printing" process for preparing uniaxial compression and cyclic loading specimens, after demolding the specimens were cured until 28 days age.

structural elements, the unusual features of the auxetic materials indicate that they could be promising for specific engineering applications such as impact resistance structure [46] and vibration mitigation structures [47,48] in the future.

In theory, the auxetic behavior of cellular materials is mainly attributed to geometrical features of the constituent material arrangement. This can be achieved by numerous designs, such as re-entrant honeycombs [49–52], rigid body rotation structures [53–55] and chiral structures [56–59]. In practice, the mechanical response varies significantly when different constituent materials are used even for the same auxetic structure. Typically, for auxetic behavior to be achieved, the constituent material should be highly elastic and deformable. If cementitious materials are to be used as constituent materials, their brittleness and low deformability need to be addressed to achieve auxetic behavior.

Previously, auxetic behavior was reported on cementitious cellular composites (CCCs) under uniaxial compression [58]. In this work, as a successive research of [58], more in depth auxetic mechanism of the CCCs was investigated and clarified. A similar ellipse shaped auxetic structure was adopted and fiber reinforced cementitious material was used as constituent material. The influence of crack bridging ability of constituent material on the mechanical behavior were subsequently analyzed. In addition, the energy dissipation ability of CCCs under cyclic loading was studied.

2. Methods and materials

2.1. Specimen preparation

Two types of specimens were fabricated for two types of tests performed. For characterizing the constituent material properties, four-point bending tests were performed. For these tests, thin bar specimens with a dimension of 160 mm × 30 mm × 10 mm were prepared.

For uniaxial compression specimens, cellular structures with

Table 1
Properties of PVA fibers used in the cementitious matrix.

Diameter	Length	Tensile Strength	Young's modulus	Density
15 μm	6 mm	1.6 GPa	34 GPa	1.28 g/cm^3

Table 2
Proportions of different constituent materials (kg/m^3).

Mix.	Cement	Fly ash	Sand (125 μm–250 μm)	Water	SP	VA	Fiber
F_0	471	556	385	428	0.86	0.3	0
F_1							12.8
F_2							25.6

repeating unit cells were designed, the total volume of the cellular structure is 67.6 cm^3. Each unit cell consists of four sections connected by four joints (e.g. Fig. 1a). Taking advantage of 3D printing technique, a so called "indirect" 3D printing technique was used. The specimen preparation procedure is as follows (shown in Fig. 1b).

- A commercial 3D printer Ultimaker 2+ was used to print the designed cellular structures using acrylonitrile butadiene styrene (ABS) as the printing material.
- The printed structures were glued in a cardboard box. A two-component silicone rubber (Poly-Sil PS 8510) (1:1 by weight) was then vacuum impregnated into the cardboard box (vacuum was kept for 1 min to remove air bubbles). The silicone rubber was left to harden for 2 h in room temperature.
- The hardened silicone rubber was detached from the printed ABS structure, resulting in a mold for creating CCC structures. These silicone rubber molds are easy to demold and durable enough for reuse.
- The mixed constituent materials were casted in the silicone mold. After 2 days the specimens are demolded from the silicone mold and then cured in saturated $Ca(OH)_2$ solution until 28 days of age.
- The specimens were painted with white acrylic paint and sprayed with red dots on the surface in order to do digital image correlation (DIC) analysis.

In this work, three mixes were used as constituent material and the mixture proportion is given in Table 2. Polyvinyl Alcohol (PVA) fibers produced by Changzhou TianYi Engineering Fiber were used as reinforcement by 0%, 1% and 2% in volume and denoted as F_0, F_1 and F_2, respectively. Physical and mechanical properties of the PVA fibers are listed in Table 1. Methylcellulose produced by Shanghai Ying Jia Industrial Development Co. Ltd. was used as viscosity modifying agent (VA) to optimize fiber distribution. Glenium 51 was used as superplasticizer (SP) to adjust mixture fluidity. The cement matrix material was a fine-grained cementitious mortar containing Portland cement (CEM I 42.5 N) and fly ash (FA) as binder materials. Tap water was used as mixing water. Water to binder ratio was set to 0.42 for all mixtures. During the casting process of the constituent material, dry materials (without fibers) were first mixed for 4 min using a Hobart machine; then, water and superplasticizer were added and mixed for 2 min; then fibers were added in and mixed for another 2 min. The total mixing time for each mixture was 8 min. The fresh mixture was cast into molds, vibrated for 40 s and covered by a plastic sheet to mitigate water loss.

2.2. Mechanical experiments

The four-point bending tests were performed on the specimens at 28 days of age. A servo hydraulic press (INSTRON 8872) was used for testing. Displacement control with a constant rate of 0.01 mm/s was used. The load was measured by the load cell and the deflection was measured by two linear variable differential transducers (LVDTs) placed at the mid-span. Five specimens were tested for each batch. The loading schematics and experimental setup are shown in Fig. 2a and Fig. 2b, respectively.

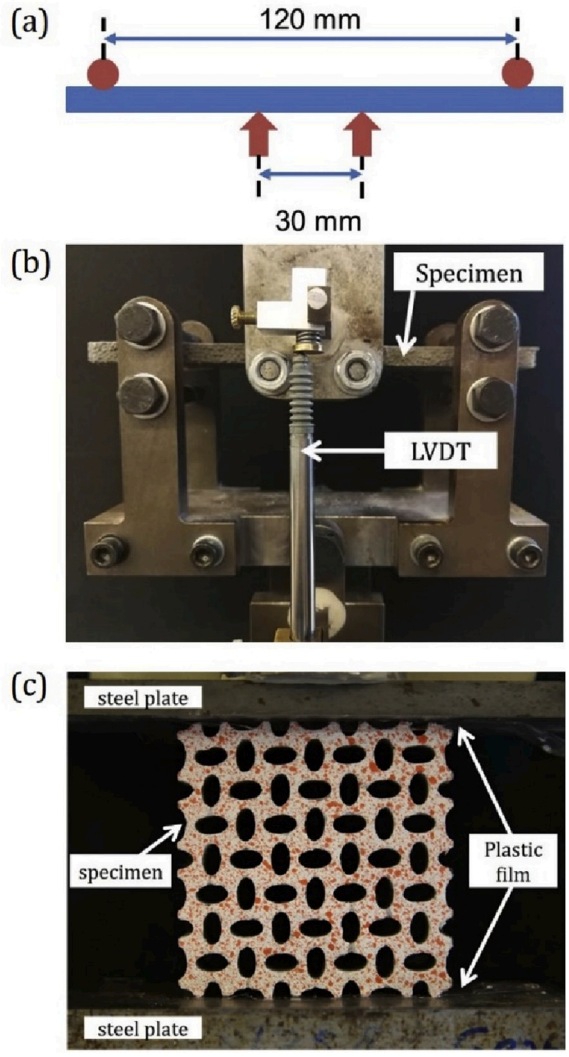

Fig. 2. (a)Schematics of four-point bending test; (b) four-point bending test setup on INSTRON 8872; (c) uniaxial compression and cyclic loading test setup on INSTRON 8872.

The uniaxial compressive test was done by a servo hydraulic press (INSTRON 8872) under displacement control, with a constant rate of 0.01 mm/s. The load and displacement are measured by the INSTRON 8872. To minimize lateral restraint at the boundaries caused by friction, plastic film was placed between the specimen and the steel loading plates at top and the bottom. The experimental setup is shown in Fig. 2c. For each test, stress-strain curve was calculated from the obtained load and displacement data, using the sample cross section 1600 mm^2 (80 mm × 20 mm) and the sample length 80 mm. The cyclic loading tests were done by the same loading setup of uniaxial compression at a constant amplitude of 2 mm and frequency of 1 Hz by a sine wave. For each cyclic loading test, 2.5×10^4 cycles were performed. Three duplicates were tested for uniaxial compression and cyclic loading test.

3. Results and discussion

3.1. Crack bridging induced auxetic behavior

As previously described, global mechanical properties of cellular materials depend on both their constituent material properties and their

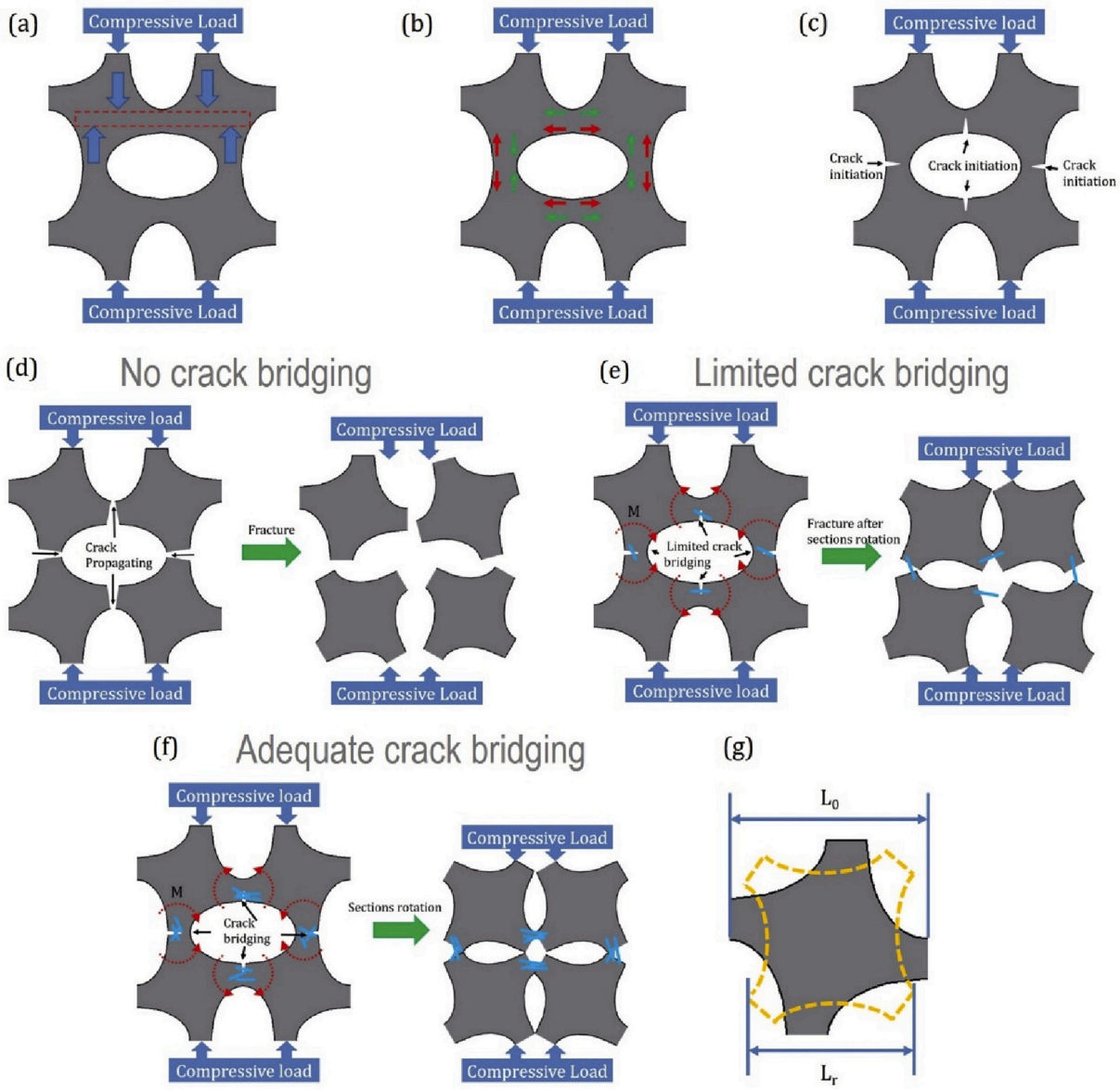

Fig. 3. Schematics of auxetic mechanism of CCCs. (a) the joints are similarly subjected to a four-point bending condition when compressive load is applied because of the chirality of each section in the single cell; (b)stress distribution at the joints after compressive load is applied, red arrow indicates tensile stress and green arrow indicates compressive stress; (c) crack initiates at the tension side of the joints, marked by black arrows; (d) the constituent material has no crack bridging ability, crack propagation leads to joints fracture, black arrows show the crack propagation direction; (e) the constituent material has limited crack bridging ability, joints separate after rotation; (f) the constituent material has adequate crack bridging ability, joints rotate without separating; (d) dimension comparison of the section in a single cell before and after rotation, $L_0 > L_r$. (For interpretation of the references to colour in this figure legend, the reader is referred to the Web version of this article.)

structural configuration. Although a similar structure was used before [37,60,61] in which local buckling is the mechanism of the auxetic behavior, for cellular structures made of cementitious materials the mechanism has not been studied yet and it is probably rather different. Therefore, prior to examining the experimental results, a theoretical analysis of the possible mechanism of CCCs exhibiting auxetic behavior will help understanding of the phenomena involved.

The proposed auxetic mechanism on the level of a unit cell is shown schematically in Fig. 3. For the cellular structure in this study, because of the chirality of the single cell section, locally the joints of each single cell are misaligned. As a result, when uniaxial compressive load is applied on the specimen, the joints are subjected to bending moment which is similar to a four-point bending condition (Fig. 3a). Consequently, tensile and compressive stresses are generated at the joints near the ends of semi-minor axis and semi-major axis of the ellipse, respectively (Fig. 3b). Since cementitious materials are much weaker in tension than in compression (compressive strength is typically 8–10 times higher than the tensile strength [62]), cracks will initiate at the tension side of the joint (Fig. 3c). Depending on the crack bridging ability of cementitious constituent materials, the crack-initiated specimen will behave differently afterwards.

If the constituent material does not have any crack bridging ability (e.g. plain mortar F_0), the crack will propagate through the joints leading to immediate fracture of the entire cellular structure; consequently, auxetic behavior will not be observed (Fig. 3d). On the other hand, if the constituent material possesses crack bridging ability, as the joints of each cell are locally subjected to bending, the sections will be able to rotate and auxetic behavior may be obtained. However, as shown in Fig. 3e, if the constituent material has limited crack bridging ability (e.g. mix F_1 with lower fiber content), the sections are only able to rotate at the beginning of the compression. As compression continues, fiber pullout can be witnessed. For the 6 mm PVA fiber used in this studied,

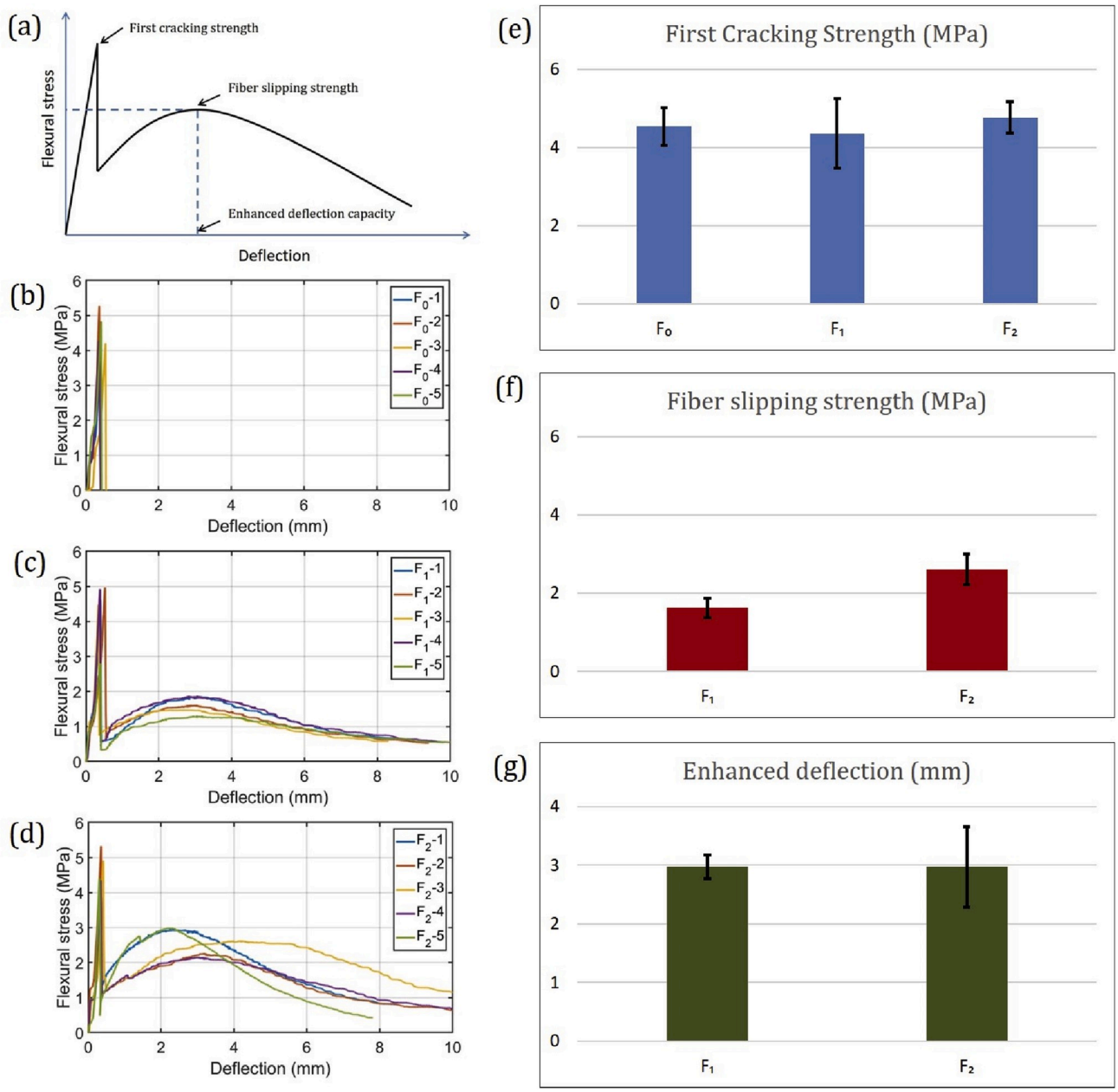

Fig. 4. (a) Several defined parameters are for the obtained flexural-deflection curves of constituent materials; (b) flexural-deflection curves of plain mortar F_0; (c) flexural-deflection curves of fiber reinfroced mortar F_1 with 1% fiber; (d) flexural-deflection curves of fiber reinfroced mortar F_2 with 2% fiber; (e) comparision of first cracking strength of three cosntituent materials; (f) comparision of fiber slipping strength of two fiber reinforced cosntituent materials F_1 and F_2; (g) comparision of enhanved deflection of two fiber reinforced cosntituent materials F_1 and F_2.

fiber embedded length varies from 0 mm to 3 mm. When crack opening increases higher than 3 mm fibers were completely pulled out. Meanwhile, some fiber still remains to bridge the crack at where the crack opening is still less than 3 mm. Eventually, some sections separate at the joints where fibers were completely pulled out. Only when the crack bridging ability is high enough (e.g. mix F_2 with higher fiber content), the joints will not fracture because of the crack bridging and the sections will be able to rotate during the entire compression until the joints are compressed together; then, eventually, the ellipse structure will disappear (Fig. 3f). Because the length in the lateral direction of a fully rotated section (L_r) is shorter than the length before rotation (L_0, see Fig. 3g), globally the specimen will exhibit lateral contraction when compressed and auxetic behavior will be obtained in this case.

According to the proposed mechanism, for the structures used in this study, the crack bridging ability of the constituent material is crucial for achieving auxetic behavior. This was evaluated by four-point bending tests in this work. A flexural-deflection curve is shown in Fig. 4a, first cracking strength (first peak load), fiber slipping strength (second peak load) and enhanced deflection (deflection at the second peak) and defined in this study and are marked on the curve. The flexural-deflection curves of F_0, F_1 and F_2 are shown in Fig. 4b~Fig. 4d. As expected, the F_0 specimens (Fig. 4b) show brittle fracture under flexural load: all specimens failed as soon as the first crack appeared, signified by the sudden drop after the peak load. Therefore, low deflection capacity was achieved during the test. While F_1 (Fig. 4c) and F_2 (Fig. 4d) show relatively higher ductility comparing to F_0: after the first crack instead of immediate rupture the load increased again and a second peak load was achieved afterwards as a result of fibers presence. As shown in Fig. 4e, because F_0, F_1 and F_2 used the same cementitious matrix, no significant difference in the first cracking strength (4.8 MPa, 4.4 MPa and 4.5 MPa

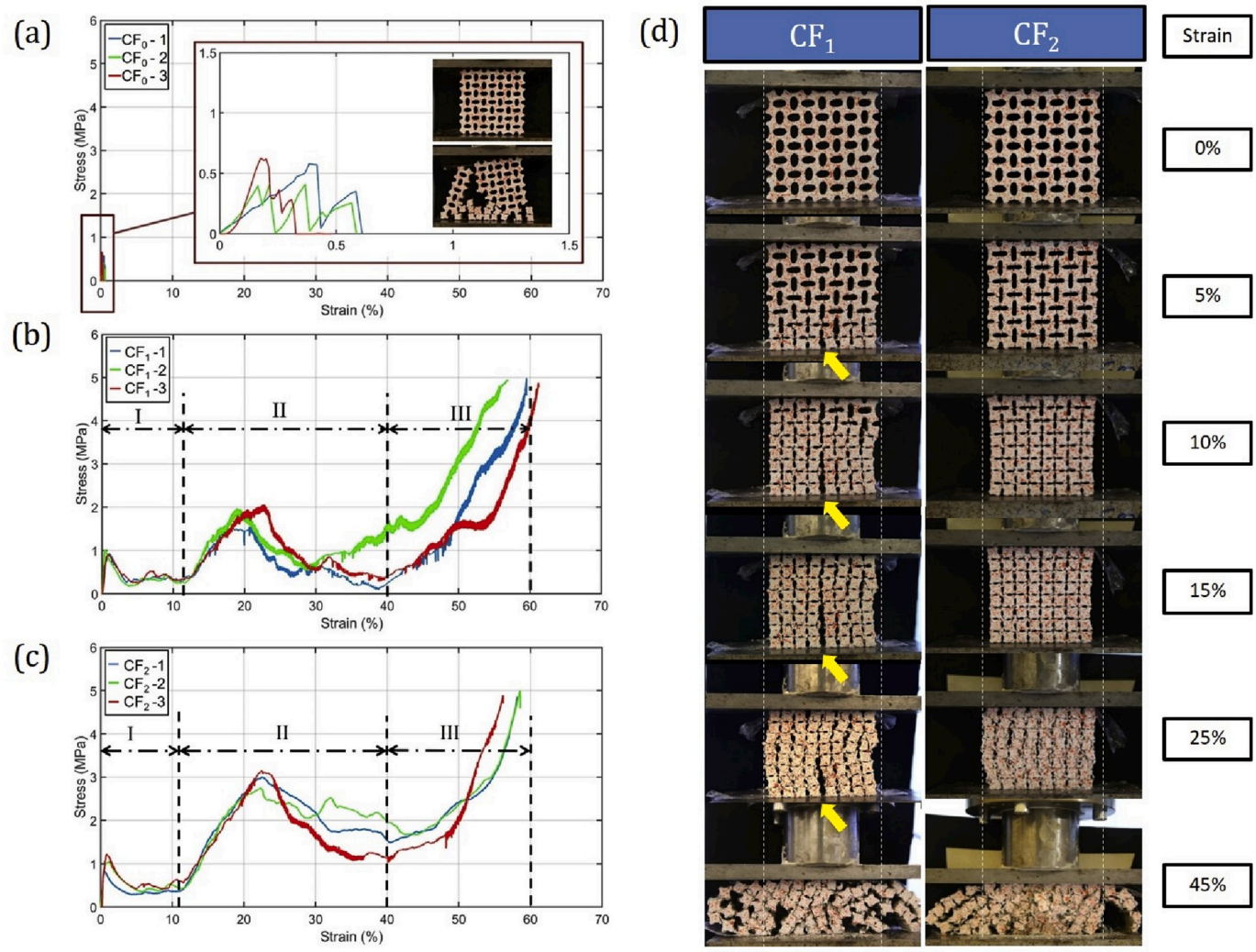

Fig. 5. (a)stress-strain curves of CCCs with F_0 as constituent material; (b)stress-strain curves of CCCs with F_1 as constituent material, three stages are marked by dashed lines; (c) stress-strain curves of CCCs with F_2 as constituent material, three stages are marked by black dashed lines; (d) comparison of the compression process at different strain level of CCCs with F_1 and F_2 as constituent materials, separated joints can be found on CF_1 specimen and marked by yellow arrows. (For interpretation of the references to colour in this figure legend, the reader is referred to the Web version of this article.)

for F_0, F_1 and F_2 respectively) was found. For F_1 (Fig. 4c)and F_2 (Fig. 4d), after the first crack instead of immediate rupture the load increased again and a second peak load was achieved afterwards. This secondary rise phenomenon can be explained by the bonding characteristics between PVA fibers and the cementitious matrix [63–65]: when applied load is high enough to violate the chemical bond between PVA fibers and cementitious matrix, fibers started to de-bond and generally be pulled out from the matrix. During the pulling out process, a so called "fibrillation" [63,65,66] process of the fiber surface appears which means that small fiber branches occurred on the fiber surface because of the damage of the PVA fibers. The presence of the branches on the fiber surface creates jamming effect at the fiber-matrix interface resulting in frictional bond effectively increases during the pulling out process, usually this process is defined as slip-hardening behavior. For F_2, higher fiber volume provided higher friction load from fiber slipping during the bending tests, resulting in a fiber slipping strength (Fig. 4f) of 2.6 MPa, compared to 1.6 MPa of F_1. However, the enhanced deflection capacity (Fig. 4g) of these two mixes is similar (about 2.9 mm). The difference in fiber slipping strength is an important indicator of the compressive behavior of CCC_S made with different constituent materials and this will be discussed in detail later in section 3.2.

3.2. Auxetic behavior of CCCs under uniaxial compression

Fig. 5 shows the stress-strain curves and the compression process of the CCCs. CCCs with F_0, F_1 and F_2 as constituent materials are denoted as CF_0, CF_1 and CF_2 respectively. As can be seen from Fig. 5a, CF_0 specimens show brittle fracture during the compression tests: after the peak load was reached, micro cracks rapidly localized which eventually lead to the failure of the compressed specimen, witnessed by a sharp drop in the stress-strain curve. Owing to the cellular structure, in some cases cracks developed through the cellular structure layer by layer so that multiple sharp drops can be found on the stress-strain curves.

Similar to the 7 days results reported in Ref. [58], the compression behavior of specimens with fiber reinforced cementitious constituent materials (F_1 and F_2) at 28 days can be also roughly divided into three stages, marked as "I", "II" and "III" on the stress-strain curves in Fig. 5.

In stage "I"(from 0% strain to roughly 11% strain), the mechanical response under compression is similar to conventional cementitious materials [62]: an ascending branch can be found as compressive load applied on the specimen, after the elastic regime micro cracks started to initiate; as soon as peak load was reached (around 1 MPa), micro cracks started to localize at the joints of individual cells. For the CF_2 specimens, owing to the fiber bridging effect, localized small cracks at the joints

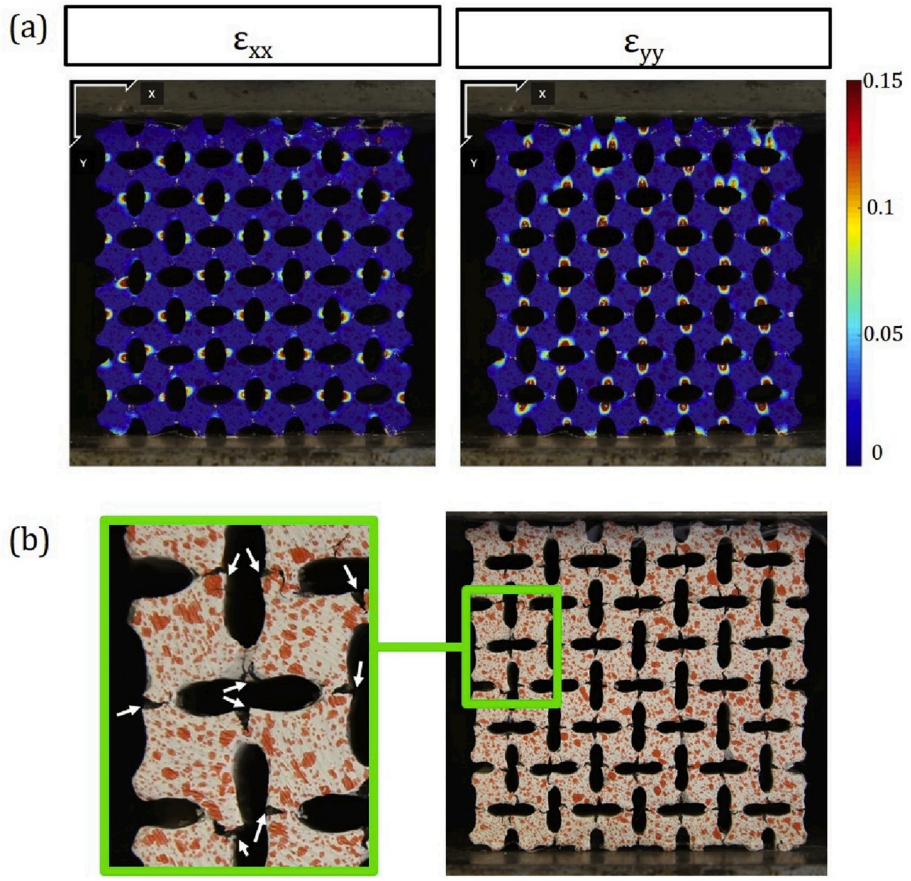

Fig. 6. (a) shows high local strain area of the CF_2 specimen at 5% strain on both ε_{xx} and ε_{yy} direction; (b) magnification of a single cell at 5% compressive strain, white arrows indicate the location of initiated cracks.

opened slowly as compression went on. As a result, the sections of individual cells started to rotate. Meanwhile, lateral contraction could be observed during the test (see Fig. 5d): auxetic behavior was achieved in this stage. As can be seen from the DIC results of CF_2 at 5% strain in Fig. 6a, the areas with high local strain which indicates that the crack initiation location are at the joints near the ends of minor axis in each ellipse structure. Because the external load was applied vertically, it also can be seen from the DIC results that the local strain at the horizontal direction (ε_{xx}) is higher than that of vertical direction (ε_{yy}) at the same global strain level. As explained in Fig. 3, the joint rotation contributed to the auxetic behavior of CCCs under uniaxial compression. As assumed in the previous section, after crack appeared fiber bridging ability of the constituent material started to dictate and contributed to prevent the joints from separating. Comparatively, for CF_1 although auxetic behavior was observed during the tests, separated joints can be found (separated joints in the middle bottom of the specimen are clearly shown in Fig. 5d, marked by yellow arrows).

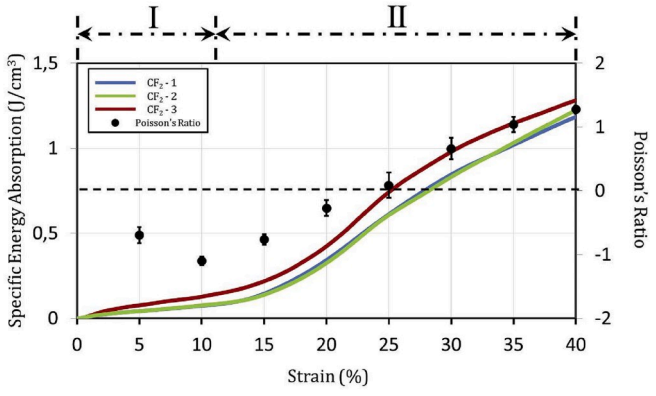

Fig. 7. Accumulative specific energy absorption of CF_2 (left y axis) and Poisson's Ratio (right axis) at different strain level for both figures stages are indicated by dashed lines, standard deviation are indicated for Poisson's ratio value.

Stage "II" (from 11% strain to 40% strain) can be recognized as compacting process of the cellular structure and subsequently failure process of the compacted "solid" material. It can be seen from Fig. 5d that as a consequence of the rotation of the single cell sections, the hollow ellipse structure was generally compacted. More contraction in the lateral direction can be observed when the vertical compression is continued. In other words, the cellular structure was destroyed during this process. Correspondingly, for both CF_1 and CF_2 that in the stress-strain curves (Fig. 5b and c) strain hardening behaviors witnessed by a load increase can be observed. This is because the cellular structure was compressed and the sections touched each other eventually. As a result, the compacted "solid" material started to bear the increasing load. Similar strain hardening process can be also found in other auxetic materials [67–69]. After the secondary peak was reached (around 2 MPa for CF_1 and 3 MPa for CF_2; because of the joints separating, the secondary peak load of CF_1 is lower) cracks started to initiate and localize in the sections of individual cells and then eventually developed to be crack planes, represented in the stress-strain curves by a descending branch after the secondary peak. In this sense, it is quite similar to the typical compression process of conventional solid fiber reinforced cementitious material.

One feature of the curve in stage "II" is very interesting: normally for solid cementitious materials, the elastic behavior regime is within one

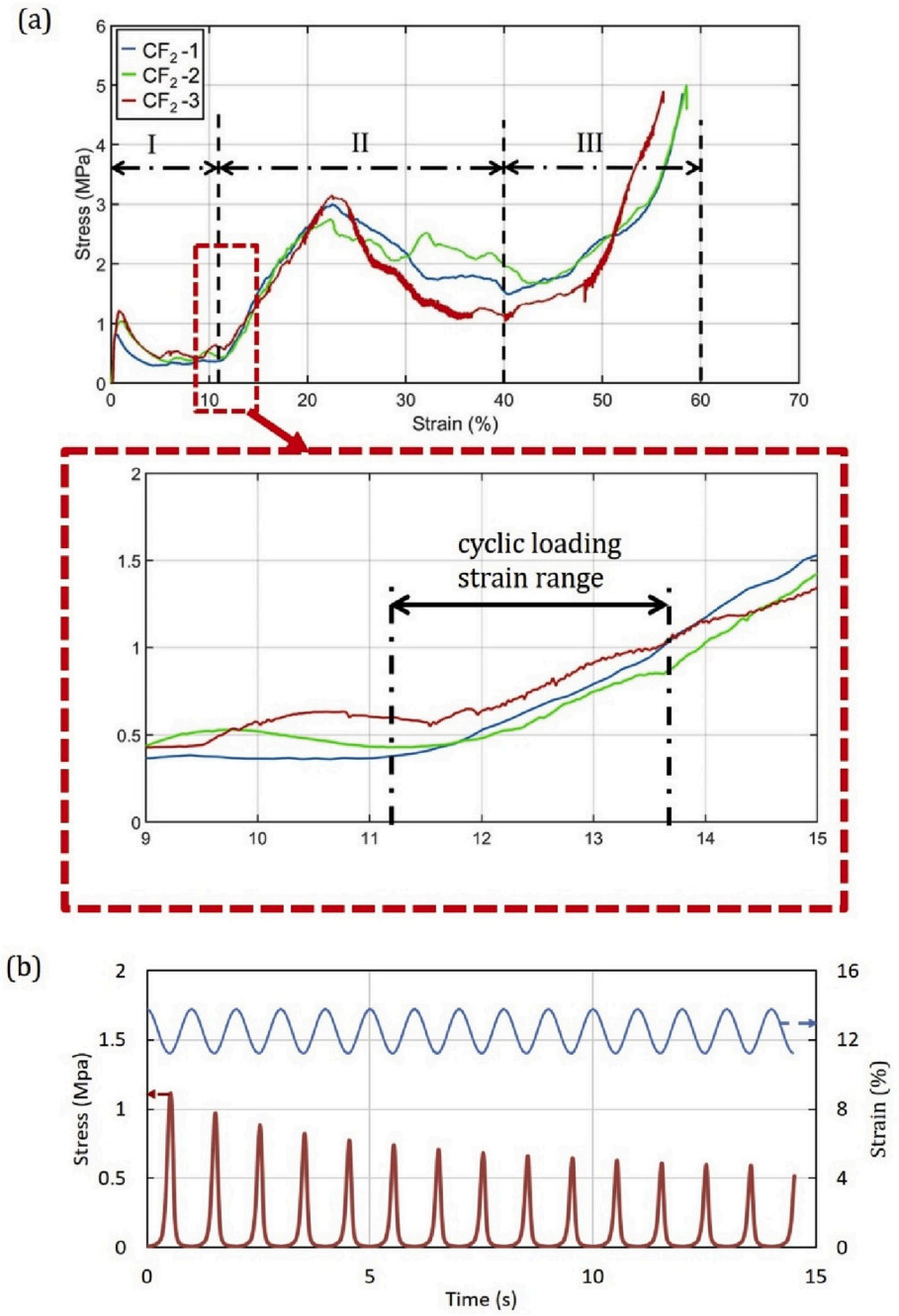

Fig. 8. (a)cyclic loading range in the secondary rise, magnified on the stress-strain curves of CF_2 within the red window; (b) stress-time curve in red and strain-time curve in blue at the beginning several cycles. (For interpretation of the references to colour in this figure legend, the reader is referred to the Web version of this article.)

third of the peak load. As the curve of CCC in stage "II" resembles solid cementitious materials, it is also reasonable to assume that CCC also behaves elastically during this regime in stage "II". This was verified by cyclic loading tests which discussed in detail in the next section.

Stage "III" (after 40% strain) is a pure compacting process of the crushed constituent material which leads to rapid stress rise because the materials were compacted denser. Similar phenomenon is mentioned in a thought experiment by van Mier [62].

From the results presented above, only CF_2 show auxetic behavior within all tested specimens. The Poisson's ratio of CF_2 was calculated using the displacement at the middle height of the specimen as lateral contraction. Fig. 7 shows the Poisson's ratio of CF_2 at different strain levels (only data before stage "II" is taken into consideration as stage "III" is the compression process of crushed debris). Negative Poisson's ratio from the beginning of the compression is found. As compressive load increased, the lowest Poisson's ratio was reached at 10% strain in stage "I". In stage "II" the Poisson's ratio started to increase indicating that several sections of individual cells started to touch each other and cracks began developing in the sections as a result. Considering the geometry of the designed structure, there is an auxetic strain limit (20%) for the CCCs to show negative Poisson's ratio which usually exists in open cell auxetic foams [70].

As a consequence of the section's rotation accompanied by fiber pulling out of the CCCs, negative Poisson's ratio is achieved for the CCCs. One probable advantage for these CCCs with auxetic behavior is their potential for high energy absorption efficiency as found in many

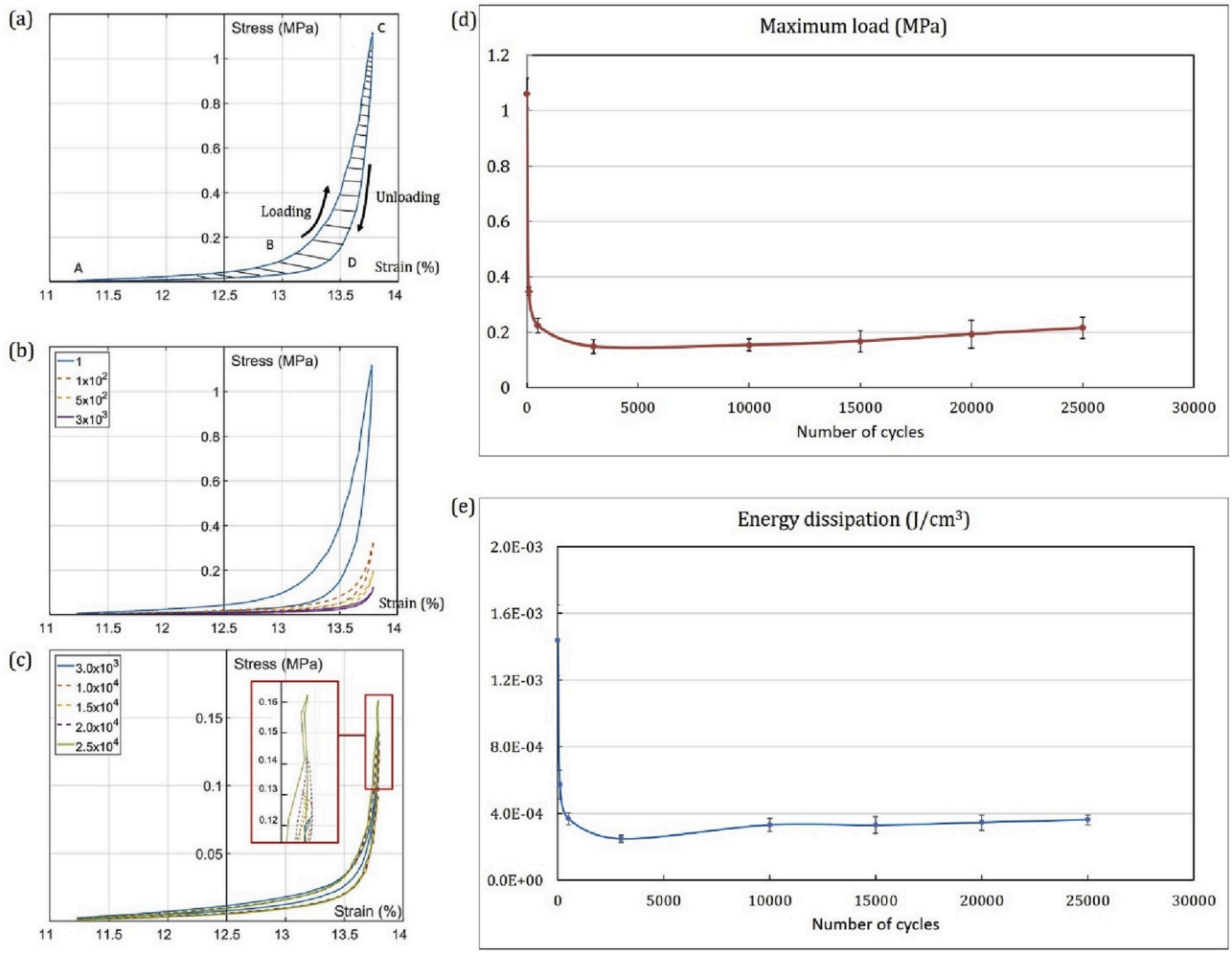

Fig. 9. (a)stress-strain curve of the first cycle, loading and unloading direction is indicated by black arrow; (b) stress-strain curves of the 1–3000 cycles; (c) stress-strain curves of the 3000–25,000 cycles, the maximum load area is magnified within the red window; (d) maximum load versus cycle numbers, standard deviation is indicated; (e) energy dissipation versus cycle numbers, standard deviation is indicated. (For interpretation of the references to colour in this figure legend, the reader is referred to the Web version of this article.)

other auxetic cellular materials. Fig. 7 shows the accumulative specific energy absorption of CF_2 at different strain. The specific energy absorption is calculated using the area under the stress-strain curves of CF_2 divided by the specimen volume. For the same reason as Poisson's ratio, stage "III" is not included in the calculation. During stage "I", the specific energy absorption increases slowly. While, after the first peak owing to the rotation of the sections, ellipse shape generally disappeared and sections came into contact. In this case, the energy absorption started to increase rapidly roughly at 10% strain which also corresponds to the strain level with the lowest Poisson's ratio. The reason is that the cellular structure of CF_2 is compacted and the sections in each single cell started to bear load leading to a secondary rise in the stress-strain curve as describe before.

3.3. Behavior of CCCs under cyclic loading

As mentioned previously, CF_2 specimens may have an "elastic" regime in stage "II" from the beginning until one third of the peak load within this stage. So, CF_2 specimens were also submitted to cyclic loading within the presumable elastic range in stage "II" from 11.25% strain to 13.75% strain (one third displacement of the peak load, see Fig. 8a). In order to reach this range, the specimens were first pre-compressed from 0% strain to 12.5% strain by 0.01 mm/s which is the same as the uniaxial compression tests and then subjected to cyclic loading with a constant amplitude of 2.5% strain (2 mm) and frequency of 1 Hz by a sine wave. The curve of stress versus time and strain versus time at the beginning several cycles is also shown in Fig. 8b.

According to the previous discussion, the tested CCCs exhibit auxetic behavior and they are efficient in energy absorption under quasi-static uniaxial compression. However, more importantly, much energy can be dissipated if CCCs behaves flexibly under cyclic loading. The stress-strain curve of CF_2 under cyclic loading at the first cycle is shown in Fig. 9a~c. As can be seen from the curve, the cyclic loading curve shows a typical hysteresis behavior: the loading branch A-B-C and unloading branch C-D-A do not overlap in one cycle. From Fig. 9b and d, it can be seen that the maximum load of each cycle dropped rapidly at the first 3000 cycles (from around 1.3 MPa–0.18 MPa) which indicates the fatigue damage of the constituent material in those contacted sections and more small cracks may appear in those sections. However, after 3000 cycles the maximum load increased again slowly with the increasing number of cycles (from 0.18 MPa to 0.22 MPa, see Fig. 9c and d). A similar trend can be also observed from the specific dissipated energy in one cycle (calculated by the area of shaded region surrounded by the loading and unloading branch in each cycle and divided by the specimen volume, see Fig. 9e). The energy dissipation decreased rapidly at the beginning followed by a gradual increase after 3000 cycles. This phenomenon is rather interesting, as explained before fibrillation of PVA fibers causes slip-hardening behavior when fibers are pulled out from

cementitious matrix. Similarly, fibrillation of PVA fiber under cyclic loading may generate more small fiber branches [71] and more jamming effects at the fibers-matrix interface can be present which may be the reason of load and energy dissipation increase after 3000 cycles. The energy dissipation in each cycle is around 4.0×10^{-4} J/cm^3 from 3000 cycles to 2.5×10^4 cycles which is rather high as an auxetic material comparing to other auxetic materials [36,72,73]. In general, the developed CCCs possessed pseudo-elasticity of 2.5% reversible strain even after 2.5×10^4 cycles, which means that the CCCs is a promising energy dissipating material.

4. Conclusions

In the present work, cementitious cellular composites (CCCs) with auxetic behavior are developed and fabricated with the aid of 3D printing. Mechanical properties of CCCs are evaluated under uniaxial compression and cyclic loading. Influence of crack bridging ability of constituent material on the mechanical behavior of CCCs are studied. Based on the obtained experimental results several conclusions can be drawn:

- During the compression process of fiber reinforced CCCs, sections rotation is observed accompanied by fiber pulling out at the joints of each single cell. As a consequence, auxetic behavior is achieved for the fiber reinforced CCCs.
- The auxetic behavior of CCCs is induced by crack bridging effect of constituent fiber reinforced cementitious material. Only when fiber slipping strength is high enough auxetic behavior can be obtained while no separated cells will be found. For the studied constituent materials in this work, 2% PVA fibers (which gives 2.6 MPa of fiber slipping strength) is enough while 0% (no fiber slipping strength) and 1% of PVA fibers (with fiber slipping strength of 1.6 MPa) is inadequate.
- Under uniaxial compression, a strain limit of auxetic behavior is found for tested specimens in this work. CF_2 has a strain limit of 20% to exhibit negative Poisson's ratio. Owing to the rotation of the sections in each single cell, sections contact increases as the compression continues, making CF_2 show strain hardening behavior under compression.
- For the developed CCCs (CF_2), a pseudo-elastic regime is found between 11.25%–13.75% strain (in total 2.5% compressive deformation). In 2.5×10^4 cycles, within this regime, CF_2 shows flexible behavior and excellent energy dissipation property.
- The fatigue damage of CF_2 is unique during the cyclic loading process: at the first 3000 cycles, fatigue damage on the cementitious matrix is significant which is indicated by the rapid drop of the maximum load. Afterwards, the maximum load starts to increase again. A corresponding trend is also found on the energy dissipation in each cycle as well. The regain in maximum load and energy dissipation implies that CCCs is possible to recover fatigue damage under cyclic loading simultaneously. A possible reason of this phenomenon could be the fibrillation of PVA fibers under numerous cyclic loads.

To the best of the authors' knowledge, this is the first time that auxetic behavior has been observed in cementitious materials. The energy dissipation ability of the developed CCCs make it very promising in engineering applications such as energy harvesting or vibration damping systems. Still, the properties such as of the developed CCCs can be improved by modifying the cellular structure and constituent material. Relevant research will be done in the future.

Declaration of competing interest

The authors declare no conflict of interest.

Acknowledgement

Yading Xu and Hongzhi Zhang would like to acknowledge the funding supported by China Scholarship Council (CSC) under the grant CSC No.201708110187 and No.201506120067. The authors would like to acknowledge Mr. Jorick Wolbert for his support in the specimen preparation and mechanical tests.

References

[1] A. Bougara, C. Lynsdale, N.B. Milestone, The influence of slag properties, mix parameters and curing temperature on hydration and strength development of slag/cement blends, Construct. Build. Mater. 187 (2018) 339–347.
[2] C. Herrera-Mesen, R.P. Salvador, S.H.P. Cavalaro, A. Aguado, Effect of gypsum content in sprayed cementitious matrices: early age hydration and mechanical properties, Cement Concr. Compos. 95 (2019) 81–91.
[3] F. Lavergne, R. Belhadi, J. Carriat, A.B. Fraj, Effect of nano-silica particles on the hydration, the rheology and the strength development of a blended cement paste, Cement Concr. Compos. 95 (2019) 42–55.
[4] I. Rahmouni, G. Promis, A. R'mili, H. Beji, O. Limam, Effect of carbonated aggregates on the mechanical properties and thermal conductivity of eco-concrete, Construct. Build. Mater. 197 (2019) 241–250.
[5] J.Y. Yoon, J.H. Kim, Mechanical properties of preplaced lightweight aggregates concrete, Construct. Build. Mater. 216 (2019) 440–449.
[6] H. Savastano Jr., S.F. Santos, M. Radonjic, W.O. Soboyejo, Fracture and fatigue of natural fiber-reinforced cementitious composites, Cement Concr. Compos. 31 (4) (2009) 232–243.
[7] D.Y. Yoo, N. Banthia, Mechanical properties of ultra-high-performance fiber-reinforced concrete: a review, Cement Concr. Compos. 73 (2016) 267–280.
[8] D.P. Bentz, C.F. Ferraris, M.A. Galler, A.S. Hansen, J.M. Guynn, Influence of particle size distributions on yield stress and viscosity of cement–fly ash pastes, Cement Concr. Res. 42 (2) (2012) 404–409.
[9] A. Abrishambaf, M. Pimentel, S. Nunes, Influence of fibre orientation on the tensile behaviour of ultra-high performance fibre reinforced cementitious composites, Cement Concr. Res. 97 (2017) 28–40.
[10] M. Amario, C.S. Rangel, M. Pepe, R.D. Toledo Filho, Optimization of normal and high strength recycled aggregate concrete mixtures by using packing model, Cement Concr. Compos. 84 (2017) 83–92.
[11] L.G. Li, C.J. Lin, G.M. Chen, A.K.H. Kwan, T. Jiang, Effects of packing on compressive behaviour of recycled aggregate concrete, Construct. Build. Mater. 157 (2017) 757–777.
[12] Y. Sun, Z. Wang, Q. Gao, C. Liu, A new mixture design methodology based on the Packing Density Theory for high performance concrete in bridge engineering, Construct. Build. Mater. 182 (2018) 80–93.
[13] M.H. Zhang, J. Islam, S. Peethamparan, Use of nano-silica to increase early strength and reduce setting time of concretes with high volumes of slag, Cement Concr. Compos. 34 (5) (2012) 650–662.
[14] A. Keulen, Q.L. Yu, S. Zhang, S. Grünewald, Effect of admixture on the pore structure refinement and enhanced performance of alkali-activated fly ash-slag concrete, Construct. Build. Mater. 162 (2018) 27–36.
[15] X.F. Wang, Y.J. Huang, G.Y. Wu, C. Fang, D.W. Li, N.X. Han, F. Xing, Effect of nano-SiO2 on strength, shrinkage and cracking sensitivity of lightweight aggregate concrete, Construct. Build. Mater. 175 (2018) 115–125.
[16] M. Qiao, J. Chen, C. Yu, S. Wu, N. Gao, Q. Ran, Gemini surfactants as novel air entraining agents for concrete, Cement Concr. Res. 100 (2017) 40–46.
[17] F. Özcan, M.E. Koç, Influence of ground pumice on compressive strength and air content of both non-air and air entrained concrete in fresh and hardened state, Construct. Build. Mater. 187 (2018) 382–393.
[18] J. Yu, J. Lin, Z. Zhang, V.C. Li, Mechanical performance of ECC with high-volume fly ash after sub-elevated temperatures, Construct. Build. Mater. 99 (2015) 82–89.
[19] C. Lu, V.C. Li, C.K. Leung, Flaw characterization and correlation with cracking strength in Engineered Cementitious Composites (ECC), Cement Concr. Res. 107 (2018) 64–74.
[20] M. Lei, C.M. Hamel, C. Yuan, H. Lu, H.J. Qi, 3D printed two-dimensional periodic structures with tailored in-plane dynamic responses and fracture behaviors, Compos. Sci. Technol. 159 (2018) 189–198.
[21] B.G. Compton, J.A. Lewis, 3D-printing of lightweight cellular composites, Adv. Mater. 26 (34) (2014) 5930–5935.
[22] Y. Xu, H. Zhang, B. Šavija, S.C. Figueiredo, E. Schlangen, Deformation and fracture of 3D printed disordered lattice materials: experiments and modeling, Mater. Des. 162 (2019) 143–153.
[23] Y. Xu, B. Šavija, Development of Strain Hardening Cementitious Composite (SHCC) Reinforced with 3D Printed Polymeric Reinforcement: Mechanical Properties, Composites Part B, Engineering, 2019, p. 107011.
[24] H. Gu, M. Pavier, A. Shterenlikht, Experimental study of modulus, strength and toughness of 2D triangular lattices, Int. J. Solid Struct. 152 (2018) 207–216.
[25] C. Bonatti, D. Mohr, Large deformation response of additively-manufactured FCC metamaterials: from octet truss lattices towards continuous shell mesostructures, Int. J. Plast. 92 (2017) 122–147.
[26] C. Qiu, S. Yue, N.J. Adkins, M. Ward, H. Hassanin, P.D. Lee, M.M. Attallah, Influence of processing conditions on strut structure and compressive properties of cellular lattice structures fabricated by selective laser melting, Mater. Sci. Eng., A 628 (2015) 188–197.

[27] Z.C. Eckel, C. Zhou, J.H. Martin, A.J. Jacobsen, W.B. Carter, T.A. Schaedler, Additive manufacturing of polymer-derived ceramics, Science 351 (6268) (2016) 58–62.
[28] J. Bauer, A. Schroer, R. Schwaiger, I. Tesari, C. Lange, L. Valdevit, O. Kraft, Push-to-pull tensile testing of ultra-strong nanoscale ceramic–polymer composites made by additive manufacturing, Extreme Mech. Lett. 3 (2015) 105–112.
[29] M. Moini, J. Olek, J.P. Youngblood, B. Magee, P.D. Zavattieri, Additive manufacturing and performance of architectured cement-based materials, Adv. Mater. 30 (43) (2018) 1802123.
[30] N.A. Fleck, V.S. Deshpande, M.F. Ashby, Micro-architectured materials: past, present and future, Proc. Math. Phys. Eng. Sci. 466 (2121) (2010) 2495–2516.
[31] N.A. Fleck, X. Qiu, The damage tolerance of elastic–brittle, two-dimensional isotropic lattices, J. Mech. Phys. Solid. 55 (3) (2007) 562–588.
[32] L. Dong, V. Deshpande, H. Wadley, Mechanical response of Ti–6Al–4V octet-truss lattice structures, Int. J. Solid Struct. 60 (2015) 107–124.
[33] M.C. Messner, Optimal lattice-structured materials, J. Mech. Phys. Solid. 96 (2016) 162–183.
[34] G.N. Greaves, A.L. Greer, R.S. Lakes, T. Rouxel, Poisson's ratio and modern materials, Nat. Mater. 10 (11) (2011) 823.
[35] Y. Han, W. Lu, Evolutionary design of nonuniform cellular structures with optimized Poisson's ratio distribution, Mater. Des. 141 (2018) 384–394.
[36] R. Critchley, I. Corni, J.A. Wharton, F.C. Walsh, R.J. Wood, K.R. Stokes, A review of the manufacture, mechanical properties and potential applications of auxetic foams, Phys. Status Solidi 250 (10) (2013) 1963–1982.
[37] M. Taylor, L. Francesconi, A. Baldi, X. Liang, F. Aymerich, A novel auxetic structure with enhanced impact performance by means of periodic tessellation with variable Poisson's ratio, in: Dynamic Behavior of Materials, vol. 1, Springer, Cham, 2019, pp. 211–218.
[38] K.E. Evans, Auxetic polymers: a new range of materials, Endeavour 15 (4) (1991) 170–174.
[39] V.L. Coenen, K.L. Alderson, Mechanisms of failure in the static indentation resistance of auxetic carbon fibre laminates, Phys. Status Solidi 248 (1) (2011) 66–72.
[40] D. Photiou, N. Prastiti, E. Sarris, G. Constantinides, On the conical indentation response of elastic auxetic materials: effects of Poisson's ratio, contact friction and cone angle, Int. J. Solid Struct. 81 (2016) 33–42.
[41] L.L. Hu, M.Z. Zhou, H. Deng, Dynamic indentation of auxetic and non-auxetic honeycombs under large deformation, Compos. Struct. 207 (2019) 323–330.
[42] H.C. Cheng, F. Scarpa, T.H. Panzera, I. Farrow, H.X. Peng, Shear stiffness and energy absorption of auxetic open cell foams as sandwich cores, Phys. Status Solidi 256 (1) (2019) 1800411.
[43] C. Qi, A. Remennikov, L.Z. Pei, S. Yang, Z.H. Yu, T.D. Ngo, Impact and close-in blast response of auxetic honeycomb-cored sandwich panels: experimental tests and numerical simulations, Compos. Struct. 180 (2017) 161–178.
[44] Y. Wang, W. Zhao, G. Zhou, Q. Gao, C. Wang, Suspension mechanical performance and vehicle ride comfort applying a novel jounce bumper based on negative Poisson's ratio structure, Adv. Eng. Software 122 (2018) 1–12.
[45] J. Ju, J.D. Summers, Compliant hexagonal periodic lattice structures having both high shear strength and high shear strain, Mater. Des. 32 (2) (2011) 512–524.
[46] R.R. Madke, R. Chowdhury, Anti-impact behavior of auxetic sandwich structure with braided face sheets and 3D re-entrant cores, Compos. Struct. 236 (2020) 111838.
[47] N.D. Duc, et al., Dynamic response and vibration of composite double curved shallow shells with negative Poisson's ratio in auxetic honeycombs core layer on elastic foundations subjected to blast and damping loads, Int. J. Mech. Sci. 133 (2017) 504–512.
[48] Y.-L. Chen, X.-T. Wang, L. Ma, Damping mechanisms of CFRP three-dimensional double-arrow-head auxetic metamaterials, Polym. Test. 81 (2020) 106189.
[49] T. Mukhopadhyay, S. Adhikari, Effective in-plane elastic properties of auxetic honeycombs with spatial irregularity, Mech. Mater. 95 (2016) 204–222.
[50] K.E. Evans, A. Alderson, Auxetic materials: functional materials and structures from lateral thinking!, Adv. Mater. 12 (9) (2000) 617–628.
[51] J.X. Qiao, C.Q. Chen, Impact resistance of uniform and functionally graded auxetic double arrowhead honeycombs, Int. J. Impact Eng. 83 (2015) 47–58.
[52] L. Yang, O. Harrysson, H. West, D. Cormier, Mechanical properties of 3D re-entrant honeycomb auxetic structures realized via additive manufacturing, Int. J. Solid Struct. 69 (2015) 475–490.
[53] J.N. Grima, K.E. Evans, Auxetic behavior from rotating squares, J. Mater. Sci. Lett. 19 (17) (2000) 1563–1565.
[54] J.N. Grima, K.E. Evans, Auxetic behavior from rotating triangles, J. Mater. Sci. 41 (10) (2006) 3193–3196.
[55] J.N. Grima, V. Zammit, R. Gatt, A. Alderson, K.E. Evans, Auxetic behaviour from rotating semi-rigid units, Phys. Status Solidi 244 (3) (2007) 866–882.
[56] A. Spadoni, M. Ruzzene, Elasto-static micropolar behavior of a chiral auxetic lattice, J. Mech. Phys. Solid. 60 (1) (2012) 156–171.
[57] M.H. Fu, B.B. Zheng, W.H. Li, A novel chiral three-dimensional material with negative Poisson's ratio and the equivalent elastic parameters, Compos. Struct. 176 (2017) 442–448.
[58] M. Fu, F. Liu, L. Hu, A novel category of 3D chiral material with negative Poisson's ratio, Compos. Sci. Technol. 160 (2018) 111–118.
[59] N. Novak, L. Starčevič, M. Vesenjak, Z. Ren, Blast response study of the sandwich composite panels with 3D chiral auxetic core, Compos. Struct. 210 (2019) 167–178.
[60] X. Ren, Studies on Three-Dimensional Metamaterials and Tubular Structures with Negative Poisson's Ratio, 2017.
[61] C. Coulais, et al., Discontinuous buckling of wide beams and metabeams, Phys. Rev. Lett. 115 (4) (2015), 044301.
[62] J.G. Van Mier, Fracture Processes of Concrete, CRC press, 2017.
[63] V.C. Li, C. Wu, S. Wang, A. Ogawa, T. Saito, Interface tailoring for strain-hardening polyvinyl alcohol-engineered cementitious composite (PVA-ECC), Mater. J. 99 (5) (2002) 463–472.
[64] V.C. Li, From Micromechanics to Structural Engineering-The Design of Cementitous Composites for Civil Engineering Applications, 1993.
[65] Z. Lin, T. Kanda, V.C. Li, On Interface Property Characterization and Performance of Fiber Reinforced Cementitious Composites, 1999.
[66] A.J. Uddin, J. Araki, Y. Gotoh, M. Takatera, A novel approach to reduce fibrillation of PVA fibres using cellulose whiskers, Textil. Res. J. 81 (5) (2011) 447–458.
[67] Z. Dong, Y. Li, T. Zhao, W. Wu, D. Xiao, J. Liang, Experimental and numerical studies on the compressive mechanical properties of the metallic auxetic reentrant honeycomb, Mater. Des. (2019) 108036.
[68] K. Meena, S. Singamneni, A new auxetic structure with significantly reduced stress concentration effects, Mater. Des. 173 (2019) 107779.
[69] H. Yang, B. Wang, L. Ma, Mechanical properties of 3D double-U auxetic structures, Int. J. Solid Struct. 180–181 (2019) 13–29.
[70] Y. Jiang, B. Rudra, J. Shim, Y. Li, Limiting strain for auxeticity under large compressive Deformation: chiral vs. re-entrant cellular solids, Int. J. Solid Struct. 162 (2019) 87–95.
[71] W.S. Lyoo, W.S. Ha, In situ fibrillation of poly (vinyl alcohol) during saponification of poly (vinyl ester)(1). Chemorheological and morphological investigations of in situ fibrillation, Polymer 40 (2) (1999) 497–505.
[72] J. Ju, J.D. Summers, J. Ziegert, G. Fadel, January). Cyclic energy loss of honeycombs under in-plane shear loading, in: ASME 2009 International Mechanical Engineering Congress and Exposition, American Society of Mechanical Engineers, 2009, pp. 283–289.
[73] M. Bianchi, F.L. Scarpa, C.W. Smith, Stiffness and energy dissipation in polyurethane auxetic foams, J. Mater. Sci. 43 (17) (2008) 5851–5860.